

# JGR Space Physics

## RESEARCH ARTICLE

10.1029/2020JA028264

### Key Points:

- Magnetosphere imaging instrument/low-energy magnetosphere measurements system low-energy telescope data are analyzed to study energetic electron and ion fluxes around Saturn's low-latitude dayside magnetopause
- Energetic particles are commonly found in Saturn's magnetosheath and their flux levels depend on the energy of particles, local time, and magnetic shear angle
- The observed dawn-dusk asymmetry in the energetic particle fluxes is consistent with the magnetic curvature drift and the magnetopause shadowing effect

### Correspondence to:

K. Liou,  
[kan.liou@jhuapl.edu](mailto:kan.liou@jhuapl.edu)












### Citation:

Liou, K., Paranicas, C., Vines, S., Kollmann, P., Allen, R. C., Clark, G. B., et al. (2021). Dawn-dusk asymmetry in energetic (>20 keV) particles adjacent to Saturn's magnetopause. *Journal of Geophysical Research: Space Physics*, 126, e2020JA028264. <https://doi.org/10.1029/2020JA028264>

Received 22 MAY 2020

Accepted 2 DEC 2020

## Dawn-Dusk Asymmetry in Energetic (>20 keV) Particles Adjacent to Saturn's Magnetopause

Kan Liou<sup>1</sup> , Chris Paranicas<sup>1</sup> , Sarah Vines<sup>1</sup> , Peter Kollmann<sup>1</sup> , Robert C. Allen<sup>1</sup> , George B. Clark<sup>1</sup> , Donald G. Mitchell<sup>1</sup> , Caitriona M. Jackman<sup>2,3</sup> , Adam Masters<sup>4</sup> , Nick Achilleos<sup>5</sup> , Elias Roussos<sup>6</sup> , and Norbert Krupp<sup>6</sup> 

<sup>1</sup>The Johns Hopkins University Applied Physics Laboratory, Laurel, MD, USA, <sup>2</sup>Department of Physics and Astronomy, University of Southampton, Southampton, UK, <sup>3</sup>Dublin Institute for Advanced Studies, Dublin, Ireland, <sup>4</sup>Blackett Laboratory, Imperial College London, London, UK, <sup>5</sup>Department of Physics and Astronomy, University College London, London, UK, <sup>6</sup>Max Planck Institute for Solar System Research, Göttingen, Germany

**Abstract** Energetic particles (>~25 keV) have been observed routinely in the terrestrial magnetosheath, but have not been well studied at the magnetosheaths of the outer planets. Here we analyze energetic electrons and ions (mostly protons) in the vicinity ( $\pm 1 R_S$ ) of Saturn's magnetopause, using particle data acquired with the low-energy magnetosphere measurements system, one of the three sensors of the magnetosphere imaging instrument on board the Cassini spacecraft, during a period of ~14 years (2004–2017). It is found that energetic particles, especially ions, are also common in Saturn's magnetosheath. A clear inward (toward Saturn) gradient in the electron differential flux is identified, suggestive of magnetospheric sources. Such an inward gradient does not appear in some of the ion channels. We conclude that Saturn's magnetopause acts as a porous barrier for energetic electrons and, to a lesser extent, for energetic ions. A dawn-dusk asymmetry in the gradient of particle flux across the magnetopause is also identified, with a gradual decrease at the dawn and a sharp decrease at the dusk magnetopause. It is also found that magnetic reconnection enhanced flux levels just outside of the magnetopause, with evidence suggesting that these particles are from magnetospheric sources. These findings strongly suggest that Saturn's magnetosphere is most likely the main source of energetic particles in Saturn's magnetosheath and magnetosphere leakage is an important process responsible for the presence of the energetic particles in Saturn's magnetosheath.

### 1. Introduction

Energetic particles of tens of kilo-electronvolt (keV) have been routinely observed in the terrestrial magnetosheath since the discovery of bursts of 40–200 keV electrons by Explorer 14 (Frank & Van Allen, 1964). Observations of energetic particles in the Earth's magnetosheath often take the form of layers of isotropic energetic electrons just outside of the magnetopause (Baker & Stone, 1977a, 1977b, 1977c; Meng & Anderson, 1970, 1975), bursts of isotropic protons and electrons in the magnetosheath (Krimigis et al., 1978; Ogasawara et al., 2011; Sarris et al., 1976), and mono-hemispheric streaming of energetic protons and electrons (Cohen et al., 2016; Scholer et al., 1982; Williams et al., 1979). The presence of energetic particles in the Earth's magnetosheath is now known to be common. Historically, both the planetary magnetosphere and its bow shock are considered the major sources of magnetosheath energetic particles.

While there is a debate about the main source and mechanism of energetic particles in the terrestrial magnetosheath, it is still not known if such energetic particles are ubiquitous and can exist in other planetary magnetosheaths. Recent studies have shown that magnetopauses are “leaky” and that both ions and electrons are able to cross the boundary, into and out of the magnetosphere, with varying efficiencies at Earth (e.g., Allen et al., 2017; Allen, Livi, & Goldstein, 2016; Allen, Livi, Vines, et al., 2016; Cohen et al., 2016, 2017; Mauk et al., 2016), Jupiter (e.g., N. Krupp et al., 2002, 2004), and Saturn (e.g., Allen et al., 2018). However, the fundamental processes and efficiencies enabling particles to cross the magnetopause are still not fully understood for any planetary magnetosphere. A comparative study of energetic particles in different planetary magnetosheaths would definitely improve our understanding of the physical processes taking place at the bow shock and the magnetopause.

Saturn is the second largest planet in the solar system. It was first visited by Pioneer 11 in 1979 followed by Voyager 1 and 2 in 1980 and 1981, respectively. These encounters discovered Saturn's magnetosphere and determined the basic characteristics of the plasma environment (Bridge et al., 1981, 1982; Frank et al., 1980; Lazarus & McNutt, 1983; Richardson, 1986; Sittler et al., 1983; Wolfe et al., 1980). However, the detailed structure and dynamics of Saturn's magnetosphere was not established until the Cassini era. Observations from Cassini showed that Saturn possesses a well-defined magnetopause and a bow shock (e.g., Dougherty et al., 2005; Kanani et al., 2010; Masters et al., 2008; Pilkington et al., 2015). Some plasma processes that occur at the Earth's magnetopause have also been identified at Saturn's magnetopause, such as dayside magnetic reconnection (Lai et al., 2012; Masters, Achilleos, et al., 2012; Masters, Eastwood, et al., 2012; McAndrews et al., 2008) and Kelvin-Helmholtz (KH) vortices (Delamere et al., 2013; Masters et al., 2010). The over one decade-long period of Cassini observations has also enabled handful of statistical studies of the general characteristics of Saturn's magnetosheath plasma and energetic particle composition (e.g., Sergis et al., 2013; Thomsen et al., 2018), magnetic structure (Sulaiman et al., 2014), electromagnetic waves (Píša et al., 2018), and turbulence (Hadid et al., 2015). In particular, relating to the present interest, Sergis et al. (2013) found traces of hot ( $>$ few keV) magnetospheric water group ions (comprised of  $\text{H}_2\text{O}^+$ ,  $\text{OH}^+$ ,  $\text{O}^+$ , and  $\text{H}_3\text{O}^+$ , and denoted as  $\text{W}^+$ ) in the magnetosheath as well as in the solar wind upstream of Saturn's bow shock. Expanding upon these observations, the present study surveys energetic particle populations in Saturn's magnetosheath, concentrating on energetic particles in regions neighboring Saturn's magnetopause. This survey of energetic particles is then used to infer physical processes that enable the escape of magnetospheric particles into the magnetosheath.

## 2. Orbit, Instrumentation, and Data

The present study uses data from the Cassini mission. Cassini was launched in October 1997 and orbited Saturn from July 2004 to September 2017, spanning more than a solar cycle and sampling Saturn's magnetosphere and boundary regions over changing planetary seasons.

### 2.1. Instrument and Data Set

The main data set analyzed in this study comes from the low-energy magnetosphere measurement system (LEMMS). The LEMMS instrument, one of the three instruments comprising the magnetospheric imaging instrument (MIMI) (Krimigis et al., 2004; Mitchell et al., 2004) suite on board the Cassini spacecraft, was a double-ended telescope designed to measure the low and high energy populations separately. Here the low-energy telescope (LET) sensors C and A channel data are utilized. The LEMMS/LET-C channel measured electron differential flux in eight energy channels that cover from 0.020 to 0.900 MeV. The LEMMS/LET-A channel measured ion differential flux in nine energy channels ranging from  $\sim$ 0.027 to 4.00 MeV/q. Note that the channel A8 responds only to helium or heavier ions and will not be included in the present analysis. The full pitch-angle distribution of energetic ions and electrons was available during the first year or so of the mission, when the LEMMS stepping motor was functioning. After that period of time, rapid pitch angle sampling is only available when the spacecraft was rolling. In addition, magnetic field measurements from the magnetic field instrument (MAG) (Dougherty et al., 2004), ion composition from MIMI/Charge Energy Mass Spectrometer (CHEMS) and low-energy electrons Cassini Plasma Spectrometer/Electron Spectrometer (CAPS/ELS) (Young et al., 2004) are also used to help data interpretation.

We survey the whole LEMMS data set when Cassini was in the neighborhood of Saturn's magnetopause within one Saturn's radius. Here we will first present a case example showing over the course of one day to provide an overview and point out a few energetic particle events, followed by a statistical study of energetic particles in Saturn's magnetosheath.

### 2.2. Events on February 3, 2007

Figure 1 shows an example of Cassini observations for February 3, 2007. This particular day, which was previously studied (Arridge et al., 2016; Masters et al., 2017), is selected because it provides examples of

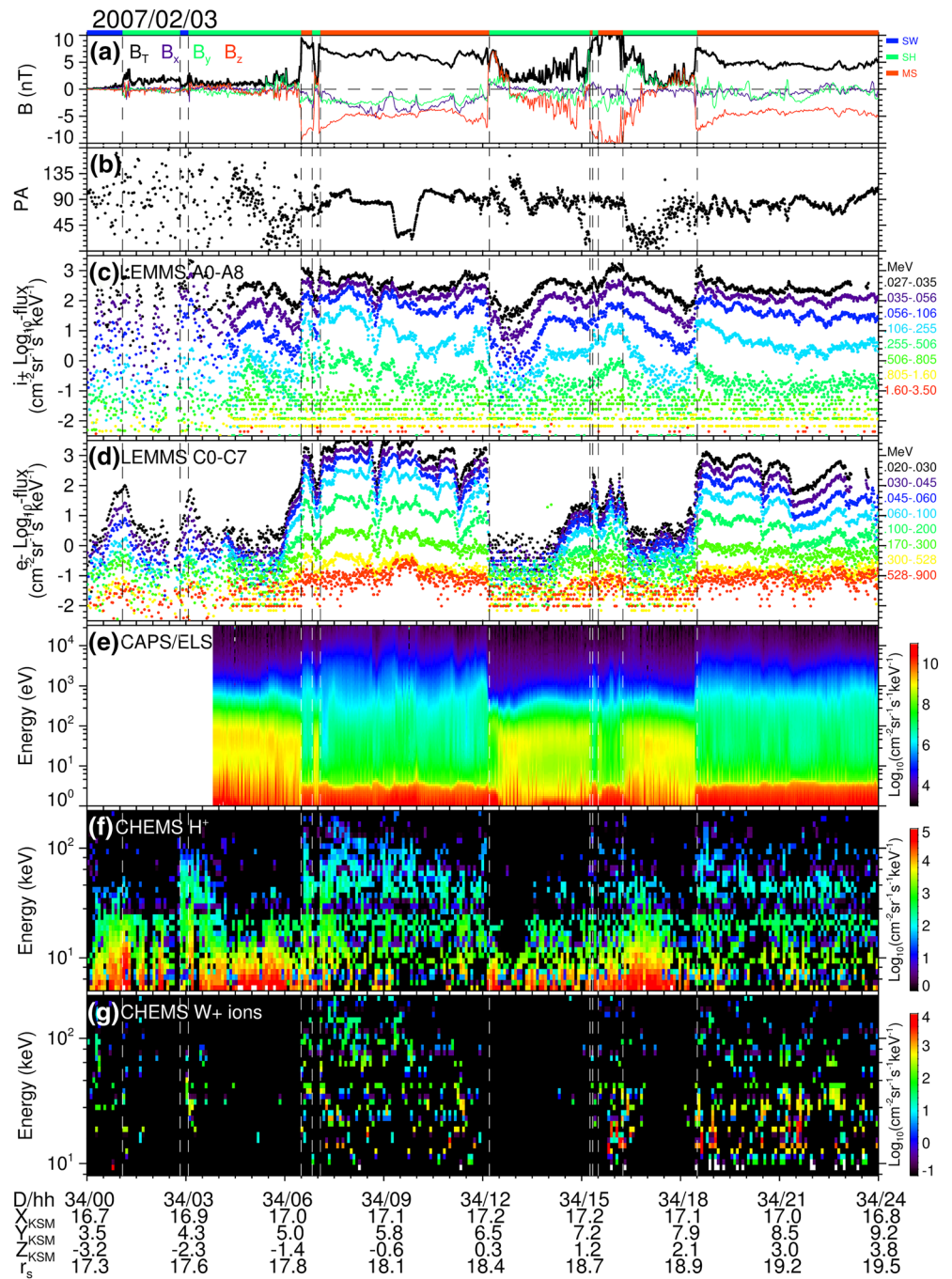


**Figure 1.** Panels from top to bottom are (a) the three components ( $B_x$ : purple,  $B_y$ : green,  $B_z$ : red) of and total ( $B_T$ : black) magnetic field from MAG, (b) pitch angle (black dots) for the LEMMS/LET-C channels, (c) proton differential flux from the LEMMS/LET-A channels, (d) electron differential flux from the LEMMS/LET-C channels, (e) electron differential flux from the CAPS/ELS sensor, (f) low-energy differential flux from the CHEMS instrument, and (g) the differential flux for water group ions from CHEMS. Vertical dashed lines mark the magnetopause. Color bars at the top indicate plasma regimes (blue: solar wind [SW], green: magnetosheath [SH], and red: magnetosphere [MS]). CAPS/ELS, Cassini Plasma Spectrometer/Electron Spectrometer; CHEMS, Charge Energy Mass Spectrometer; LEMMS, low-energy magnetosphere measurements system; LET, low-energy telescope; MAG, magnetic field instrument.

multiple magnetosheath energetic particle events in which multiple instrument datasets are available. At the beginning of this day, Cassini was near the equatorial noon region at (16.7, 3.5, -3.2)  $R_s$ , where  $R_s = 60,268$  km is the Saturn equatorial radius at 1 bar (Seidelmann et al., 2007), in the Cartesian Kronocentric solar magnetospheric (KSM) coordinate system (e.g., Dougherty et al., 2005) moving duskward and outbound. The KSM system has its  $x$ -axis pointing toward the Sun and the  $z$ -axis is the projection of Saturn's magnetic dipole axis (positive north) onto the plane perpendicular to the  $x$ -axis. The  $y$ -axis completes the right-handed triad.

Cassini made multiple encounters with the magnetopause and bow shock on this day. Because the speed of Cassini was slow near its apoapsis, consecutive crossings with a time interval less than  $\sim 1$  day are likely due to inward and outward movements of the bow shock and magnetopause. Panels in Figure 1 from top to bottom show (a) the components of the magnetic field from MAG, (b) pitch angle (black dots) for the C channels, (c) ion differential flux from the A channels, (d) electron differential flux from the C channels, (e) electron energy spectrogram from CAPS/ELS, (f) proton energy spectrogram from CHEMS, and (g) water group ion energy spectrogram from CHEMS. The distinct plasma regions encountered by Cassini are color labeled (solar wind (SW): blue, magnetosheath (SH): green, and magnetosphere (MS): red) on top of the first panel. The boundaries that separate the regions clearly coincide with sharp excursions of the magnetic field shown in Figure 1a. Measurements of these regions are also separated by vertical dashed lines. The identified plasma regions are determined by MAG magnetic field measurements and lower-energy proton measurements from CAPS/ELS and CHEMS. For CHEMS data, the normalized PHA event data are used, which are explained in the Planetary Data System user guide (Vandergriff et al., 2018). The universal time (UT) and the location, in the Cartesian KSM coordinate system, of the measurements are listed at the bottom of Figure 1.

As shown in Figure 1, this 24-h interval contains three bow shock crossings and nine magnetopause crossings. In general, similar to the terrestrial magnetosphere, Saturn's outer magnetosphere reveals a clearly detectable flux of energetic particles, with the differential flux at times reaching  $> \sim 10^3$   $\text{cm}^{-2}\text{sr}^{-1}\text{s}^{-1}\text{keV}^{-1}$  for 20–45 keV electrons and  $> \sim 10^2$   $\text{cm}^{-2}\text{sr}^{-1}\text{s}^{-1}\text{keV}^{-1}$  for 27–106 keV protons. Outside the magnetosphere, the proton differential flux was slightly smaller (by no more than one order of magnitude) but can be comparable at times. The electron differential flux outside the magnetopause was significantly smaller than in the magnetosphere, up to three orders of magnitude, depending on the energy of electrons.

At the beginning of the day, Cassini was in the solar wind. Prior to this day, Cassini was in the magnetosphere for  $\sim 8$  h starting at 15:20 UT and encountered the magnetopause at 23:30 UT and the bow shock at 23:50 UT (not shown), suggesting a quick inward movement of the magnetopause and bow shock. At  $\sim 01:05$  on day 34, Cassini moved inbound into the magnetosheath, followed by a pair of inbound-outbound bow shock crossings in quick succession at  $\sim 02:50$  UT and  $03:05$  UT, before the first magnetopause crossing of the day at  $\sim 06:30$  UT. The electron fluxes (channels C0–C7) are a good indicator for magnetospheric plasma, since electrons in the 10's of keV to MeV energy range tend to have much higher fluxes than in the solar wind and magnetosheath. McNutt et al. (2007) also found a strong increase in energetic electron fluxes passing into Jupiter's magnetosphere. During the first  $\sim 3$  h in the magnetosheath/solar wind, Cassini observed two electron bursts and 5–6 ion bursts. The peak differential flux for protons was comparable to those in the magnetosphere, whereas the peak differential flux for electrons was about one order smaller. The bursts of electron appear in all C channels with energies ranging from 0.020 to 0.900 MeV, whereas the bursts of ions can be seen only up to  $\sim 0.8$  MeV. Observations from CHEMS (Figures 1f and 1g) indicate that these bursts of energetic ions and electrons were accompanied with enhanced low energy ( $< 10$  keV) protons and traces of water group ions in the keV energy range (e.g.,  $\sim 3$  UT). Because the water group ions are believed to be mainly generated by Saturn's moon Enceladus (e.g., Smith et al., 2008), it is suggested that bursts of energetic ions are likely of magnetospheric origin.

At 06:30 UT, Cassini entered the magnetosphere. At the magnetopause, both proton and electron fluxes showed a sharp increase (by one order of magnitude or less). However, the electron flux seemed to start increasing  $\sim 30$  m earlier from its background level (e.g., a few to  $\sim 10^2$   $\text{cm}^{-2}\text{sr}^{-1}\text{s}^{-1}\text{keV}^{-1}$  for 20–30 keV electrons), mimicking a “layer” of energetic electrons just outside of the magnetopause seen at the Earth's magnetopause (e.g., Meng & Anderson, 1970). Another such layer of energetic electrons was observed near the magnetopause crossing at  $\sim 15:12$  UT. To first order approximation, the thickness of the layer can be



estimated assuming a static magnetopause during the crossing. We use the magnetopause crossing point at 06:30 UT to estimate the magnetopause location using Kanani et al.'s (2010) magnetopause model. The (shortest) distance between Cassini and the modeled magnetopause can be estimated for the time of interest. It is equivalent to converting Cassini's trajectories to a local boundary normal coordinate and the thickness is estimated along the magnetopause normal direction. The thickness (starting from 0600 to 0630 UT) of the electron layer is estimated to be  $\sim 1.96 \times 10^3$  km ( $\sim 0.03 R_s$ ). Using the averaged total magnetic field  $\sim 1.6$  nT over the 0600–0630 UT interval, the gyroradius of the lowest energy channel ( $\sim 25$  keV) electrons is  $\sim 235$  km, or  $\sim 1/8$  of the thickness of the electron layer. In addition, the electron layer's thickness does not increase with the electron energy, and thus does not seem to have a gyroradius dependence.

Now let's turn to energetic ions. The gyroradius for 30 keV ions, assuming protons and  $B = 1.6$  nT, is  $\sim 1.10 \times 10^4$  km or  $\sim 0.18 R_s$ . Again, using the magnetopause location at 06:30 UT, we estimate that Cassini would begin to see protons  $\sim 2:00$  UT or earlier for heavier ions. Therefore, a large part of ions seen prior to the 06:30 magnetopause crossing could be due to the finite gyroradius effect.

At other magnetopause crossings, for example, at 12:15 and 18:30 UT, the differences between the ion and electron fluxes inside and just outside the magnetosphere were much sharper. Comparing the magnetic field for times of sharp versus more gradual flux transitions, one can see that the magnetic field had a large northward component on the magnetosheath side of the magnetopause for the sharp transition, whereas the magnetosheath magnetic field had a small or negative  $z$ -component for the gradual transitions. Opposite to that of the Earth, the magnetic dipole at Saturn is oriented along the spin axis, resulting in the equatorial magnetic field to be directed southward. This can be seen in Figure 1a, which shows southward excursions of the  $B_z$  component in the magnetosphere. Thus dayside subsolar reconnection would be more likely to occur when the IMF (more precisely the magnetosheath field) is northward. Therefore, this suggests that a sharp flux transition for the 10's to 100's of keV electrons at the magnetopause may be associated with dayside merging. These events seem to suggest that gradual transitions have more magnetospheric loss than sharp transitions or that a thicker boundary layer has more loss than the sharp transition.

### 3. Statistical Analysis

The case study event on February 3, 2007 provides a number of interesting features about the presence of energetic particles in Saturn's magnetosheath. Because Cassini spanned a solar cycle and different seasons on Saturn, one could possibly explore a wide parameter space, such as examining local time and latitudinal effects. In order to provide insights into the physical processes that result in the leakage of Saturn's energetic magnetospheric particles into the magnetosheath, we have performed a statistical analysis of the energetic particles in Saturn's magnetosheath and magnetosphere adjacent to the magnetopause (within  $1 R_s$ ).

During the 14 years of the orbital phase of the Cassini mission from 2004 to 2017, Cassini spent a total of 793.9 days in Saturn's magnetosheath, of which 592.5 days were on the dayside and 211.4 days were on the nightside. Figure 2a shows the projection of the Cassini orbits, as well as the modeled magnetopause (Kanani et al., 2010) and bow shock (Masters et al., 2008), on the  $X$ - $Y$  plane of the KSM coordinate system. There is generally good coverage of the magnetosheath by Cassini orbits roughly from 05 to 19 LT. A list of 2118 identified magnetopause and 1,243 bow shock crossings (Jackman et al., 2019) is used to help determine the plasma regions sampled by Cassini. Figure 2b shows segments of the Cassini orbit that were identified as being in the magnetosheath, color coded by the year of the orbits. One can see that there is a dawn-dusk difference in the sampling periods. Cassini surveyed the dusk magnetosheath during 2010–2013 and the dawn magnetosheath during 2004–2007 and 2014–2017. Because solar wind structures vary with solar cycle, the sampling bias can result in different content of solar energetic particles, thus possibly affecting our interpretation. We will discuss possible effects in later sections.

We adopt the empirical model of the magnetopause of Kanani et al. (2010):

$$r = R_0 \left( \frac{2}{1 + \cos \theta} \right)^K \quad (1)$$

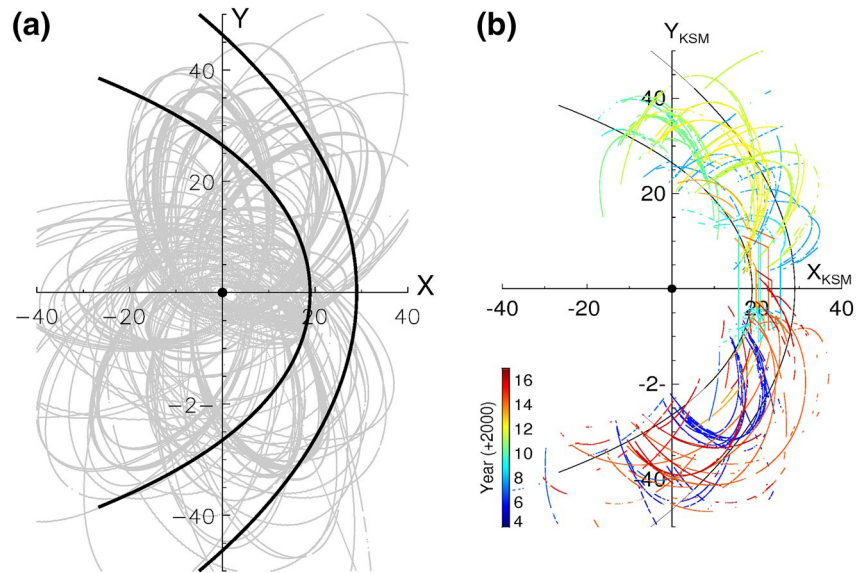


**Figure 2.** (a) Projection of Cassini orbits from 2004 to 2016 along with the projection of the modeled bow shock (Masters et al., 2008) and magnetopause (Kanani et al., 2010) in Saturn's equatorial plane, assuming the solar wind dynamic pressure  $D_p = 0.048$  nPa. (b) Line segments indicate Saturn's magnetosheath crossings (Jackman et al., 2019). The orbits are color-coded by years. The Kronocentric Solar Magnetospheric (KSM) coordinate system in units of Saturn radii is used.

where  $R_0 = a \cdot D_p^{-b}$ ,  $K = c + d \cdot D_p$ , and  $D_p$  is the dynamic pressure ( $a = 10.3 \pm 1.7$ ,  $b = 0.20 \pm 0.03$ ,  $c = 0.73 \pm 0.07$ ,  $d = 0.4 \pm 0.5$ ). This model assumes axial symmetry about the  $x$ -axis. Therefore,  $r$  is the distance from the center of Saturn to any point on the magnetopause and  $\theta$  is the polar angle of that point.

To explore energetic particle flux variations in the vicinity of the magnetopause, we perform a “distance-based” superposed analysis. In the conventional superposed epoch analysis, the magnetopause crossing time is used as the zero time. Time series of data is arranged against the zero epoch. In our distance-based superposed analysis, the location of each of the magnetopause crossings are considered as the origin and is fixed and the  $x$ -axis represents the measure of the distance from the magnetopause. The distance-based method does not necessarily provide a more accurate result than the time-based method but to better describe spatial rather than temporal variations of phenomena. To carry out this analysis, we first estimate the (shortest) distance of Cassini from the magnetopause before and after each crossing using the Kanani et al. (2010) magnetopause model to determine the boundary normal direction for each crossing. The distance is then measured along the magnetopause normal direction of the modeled magnetopause. We further limit the observations that were made within  $45^\circ$  of the equator to minimize the effect from polar flattening (Pilkington et al., 2014). The spatial domain is set to  $1 R_s$  from the magnetopause with uniform bins of  $0.01 R_s$  in size. The LEMMS/LET data is further averaged over 14–19 LT, 10–14 LT, and 05–10 LT for the dusk, noon, and dawn sectors, respectively, to increase statistics. It is important to note that the distance-based method uses a hyperbola (Kanani et al., 2010) to describe Saturn's magnetopause. In reality, Saturn's magnetopause may not be as smooth as a hyperbola as it may be modulated by the KH instability (Delamere et al., 2013; Masters et al., 2010). Observations have suggested that if the KH wavelength is  $\sim 10 R_s$ , then the KH vortex/nonlinear wave amplitude should be  $\sim 1 R_s$  (Masters, Achilleos, et al., 2012). Therefore, this may affect the present distance-based analysis.

To separate possible effects on particle leakage from different processes occurring at the magnetopause, such as magnetic reconnection, events are ordered by the magnetic shear angle ( $\theta_s$ ), the angle between magnetosheath and magnetospheric magnetic field vectors. The shear angle is estimated by averaging magnetic field over a region ( $\sim$ several minute long) in the magnetosheath and magnetosphere a few minutes away from the magnetopause to account for the finite thickness of the magnetopause and possible turbulent field associated with the magnetopause current.

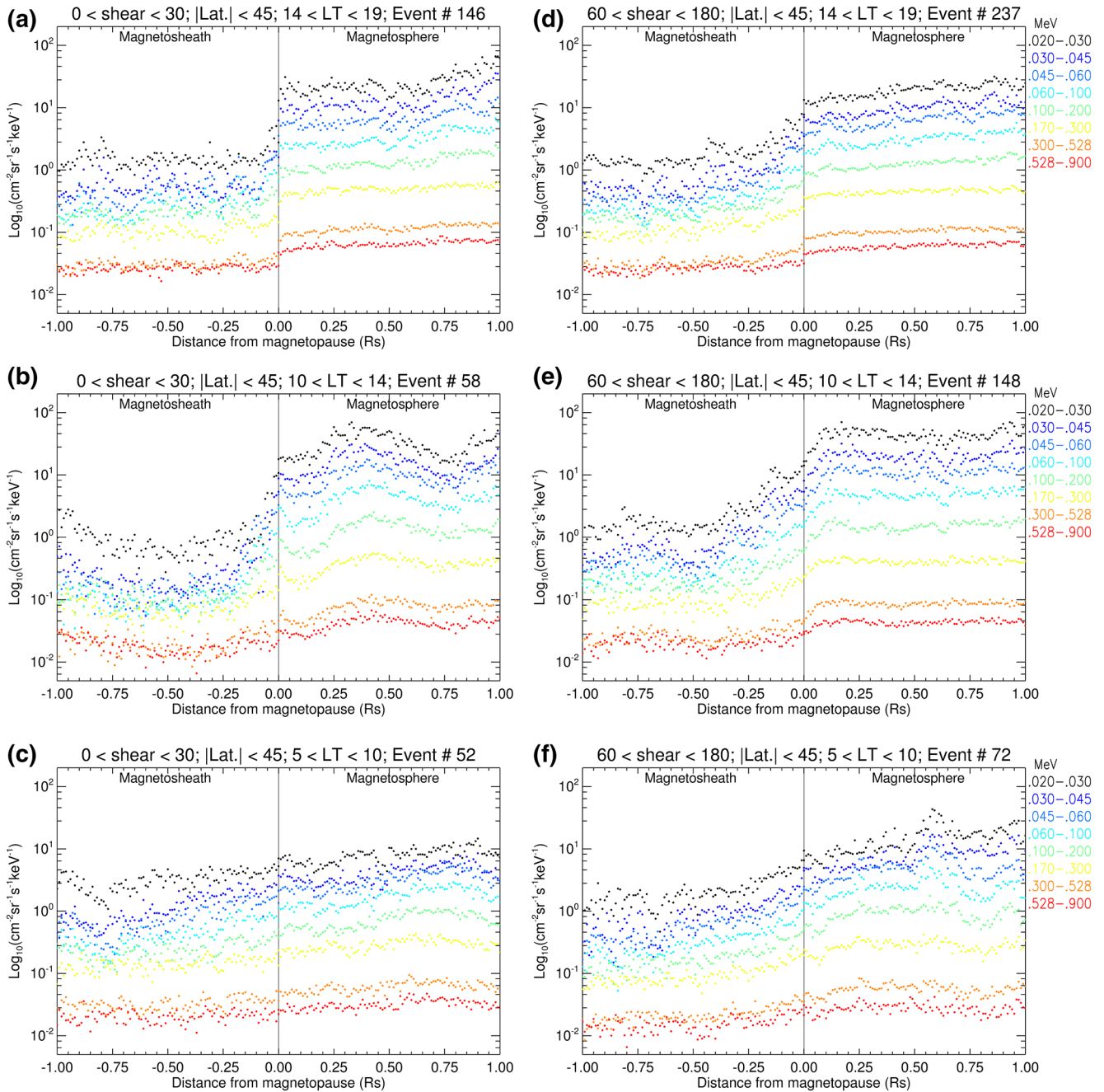


**Figure 3.** Median values of electron differential fluxes ( $\text{cm}^{-2}\text{sr}^{-1}\text{s}^{-1}\text{keV}^{-1}$ ) from LEMMS/LET-C sampled within  $45^\circ$  of latitudes in the (a) dusk (14–19 MLT), (b) noon (10–14 MLT), and (c) dawn (05–10 MLT) sectors for low-magnetic shear ( $<30^\circ$ ) conditions. In each panel, energy channels are color coded (see right inserts for each channel’s energy range). Panels on the right (d–f) have the same format as those on the left but for magnetic high-shear ( $>60^\circ$ ) conditions. The vertical line at the center of each Figure marks the location of the magnetopause.

### 3.1. Electron Differential Flux

Figures 3a–3c show the median value of electron differential fluxes from the C channels for low magnetic shear ( $\theta_s < 30^\circ$ ). The median electron flux on the magnetospheric side of the magnetopause is typically in the order of  $10^1$ – $10^2 \text{ cm}^{-2}\text{sr}^{-1}\text{s}^{-1}\text{keV}^{-1}$ . On the magnetosheath side, the flux level is smaller by  $\sim 1$  order of magnitude. There are some noticeable dawn-dusk differences in the electron flux that are worth pointing out. First, the electron flux, when averaged over the  $1 R_s$  distance from the magnetopause, is  $\sim 2$ – $3$  times higher in the dusk than in the dawn flank magnetosphere. This dawn-dusk difference is consistent with the

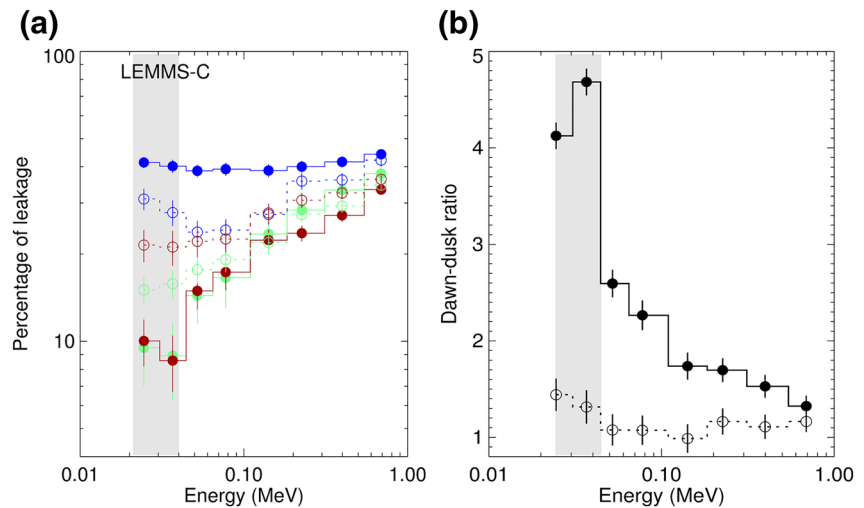


**Figure 4.** (a) Percentage of magnetospheric leak of energetic electron flux, defined as the ratio of magnetosheath to total (magnetosheath + magnetosphere) flux, for the dawn (blue), noon (green), and dusk (red) sectors. Solid lines are for low magnetic shear and dotted lines are for high magnetic shear conditions. (b) Dawn-to-dusk ratio of the leak percentage for low magnetic shear (solid lines) and high magnetic shear (dotted lines) conditions. The vertical bars represent one standard deviation of the population mean. The shaded area in each panel indicates possible light contamination.

corotation, leading both ions and electrons to encounter the dawn flank before convecting through noon to dusk. Some of these ions and electrons would then be expected to be lost to magnetopause shadowing along the dawn flank. Second, in the magnetosheath, the electron flux is larger, but only slightly (up to a factor of 2 for C0), in the dawn than in the dusk flank. Because electron fluxes within  $1 R_s$  of the magnetopause are also larger in the dusk flank for the magnetosphere, the magnetosheath-to-magnetosphere flux ratio is in general the largest at the dawn flank, followed by the noon sector and by the dusk flank, suggesting a possible dawn-dusk asymmetry in the amount of leakage of energetic particles into the magnetosheath from the magnetosphere. Third, the magnitude of the flux drops is more pronounced at the dusk than at the dawn flank.

If we assume that Saturn's magnetosphere is the primary source of energetic electrons and ignore electron transport effects, the percentage of leakage of energetic magnetospheric electrons can be defined as the ratio of the magnetosheath to total (magnetosheath + magnetosphere) flux. The leakage is calculated with the average fluxes within  $\sim 0.3 R_s$  from the magnetopause. This is because the most important variations in the sheath fluxes are confined within that distance. Figure 4a shows the percentage of leakage for the dawn (blue), noon (green), and dusk (red) sectors for low magnetic shear conditions (solid lines). In general, the percentage of leakage increases with increasing electron energies, except for the lowest energy channel (C0: 20–30 keV) electrons, ranging from  $\sim 40\%$  in the dawn flank to  $\sim 10\%$ – $35\%$  at noon and in the dusk flank. Note that low-energy channels are susceptible to light contamination. Although algorithms that remove the light contaminated counts have been developed and applied to the data, the clean-up is not perfect and some residuals may still exist, especially the two lowest-energy channel counts (the shaded area in Figure 4). Clearly, there is a dawn-dusk asymmetry in the percentage of leakage and the asymmetry is more pronounced for lower energy than for higher energy electrons (see Figure 4b, solid line), ranging from  $\sim 4.7$  for the lowest energy channel to  $\sim 1.5$  for the highest energy channel. This result is expected because higher energetic particles have a larger gyroradius and are less confined by the magnetopause.

For higher magnetic shear ( $60^\circ < \theta_s < 180^\circ$ ), the general trend for the flux changes across the magnetopause is similar to those for low magnetic shear (see Figures 3d–3f), except the flux decrease across the magnetopause is more gradual. Except for the lowest energy channel, the percentage of leakage also increases with increasing electron energy, ranging from  $\sim 20\%$  to  $40\%$  for the three local time sectors. The dawn-dusk asymmetry in the percentage of leakage seen for lower magnetic shear reduces significantly ( $< 50\%$ ), shown as the dotted line in Figure 4b.



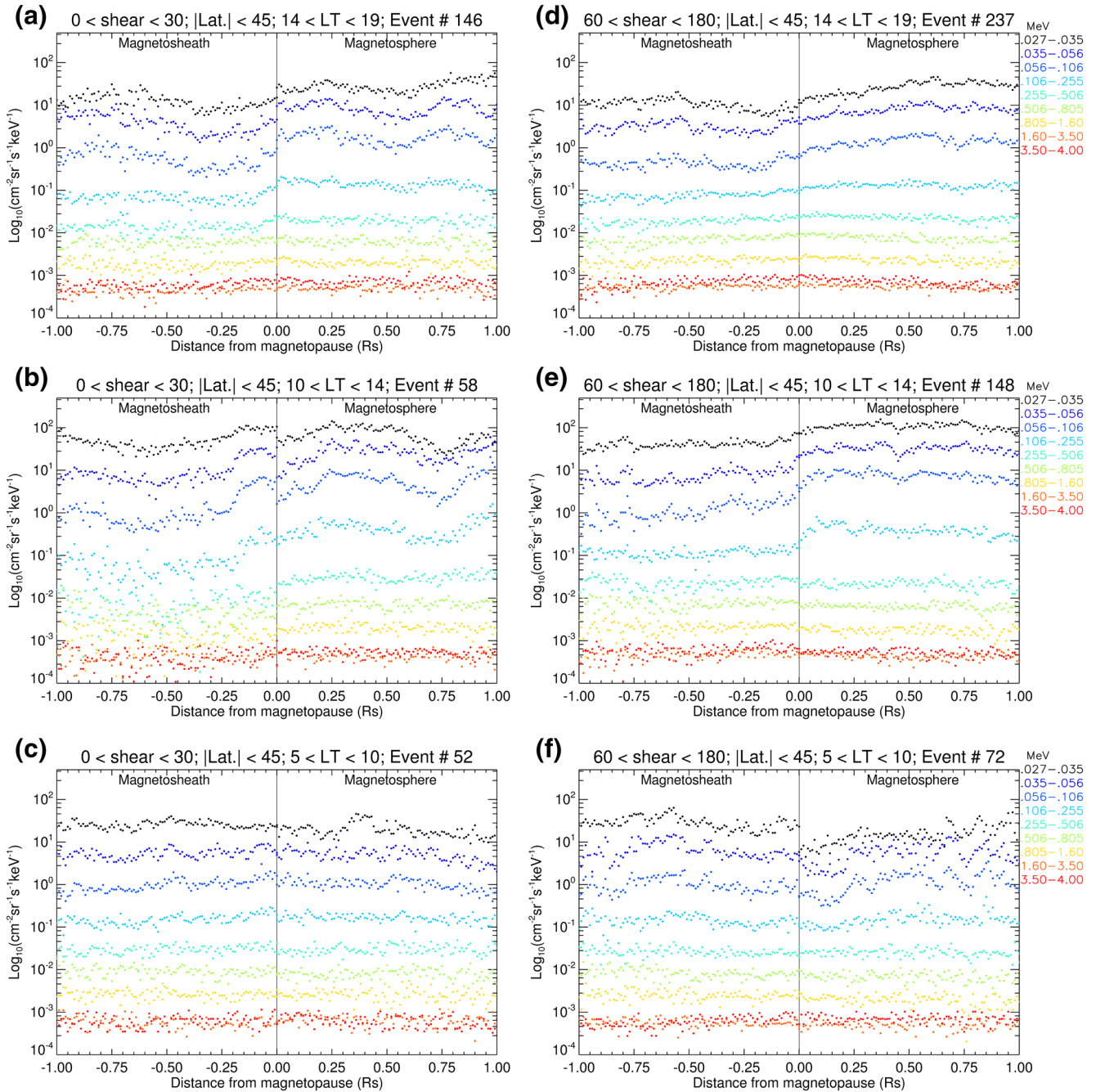


**Figure 5.** Same format as Figure 3 but for the LEMMS/LET-A channel (energetic ion flux) data. LEMMS, low-energy magnetosphere measurements system; LET, low-energy telescope.

### 3.2. Ion Differential Flux

Figures 5a–5c show the median value of ion differential fluxes from the A channels for low magnetic shear ( $\theta_s < 30^\circ$ ). The typical flux for 30 keV ions (A0; black dots) around the magnetopause is on the order of  $\sim 10^{-2}$ – $10^2$   $\text{cm}^{-2}\text{sr}^{-1}\text{s}^{-1}\text{keV}^{-1}$ , with the largest flux in the noon sector, followed by the dawn flank and then the dusk flank. The difference in the ion fluxes between the magnetosphere and the magnetosheath is less pronounced than those seen in the electron fluxes. In the dusk flank, there is a clear drop (by  $\sim 50\%$ ). The drop is more pronounced at lower energy channels and become less pronounced for higher energy ions

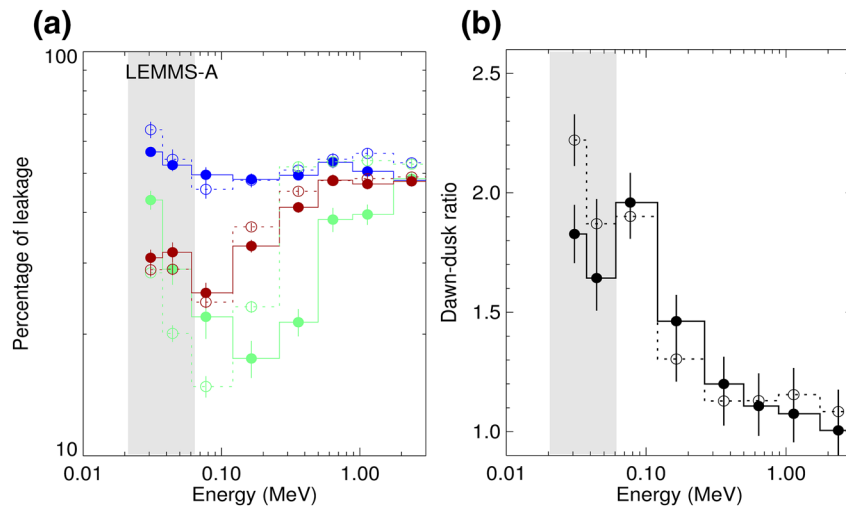


**Figure 6.** Same format as Figure 4 but derived from the LEMMS/LET-A channel (energetic ion flux) data. LEMMS, low-energy magnetosphere measurements system; LET, low-energy telescope.

(>~506 keV). In the noon sector, ion fluxes are more variables but there are still more ions in the magnetosphere than in the magnetosheath for certain energies. In the dawn flank, there is no clear flux change across the magnetopause.

For higher magnetic shear ( $60^\circ < \theta_s < 180^\circ$ ), as shown in Figures 5d–5f, the ion fluxes show a decrease across the dusk magnetopause. The decrease seems to be more gradual than those for the low shear magnetopause. There is no significant change in the ion fluxes for ions with energies greater than ~250 keV. The high shear dusk flank magnetosheath-to-magnetosphere flux ratio is less than 1 and ranges from 0.45 (channel A3, 56–106 keV) to 0.99 (channel A8, 3.5–4.0 MeV). In the noon sector, the average flux in the magnetosphere is largest among the three local-time sectors being considered. The flux ratio for A1–A4 drops gradually to a range between 0.26 (channel A2, 56–106 keV) and 0.40 (channel A0, 20–30 keV). However, for higher energy channels (>~255 keV), the flux ratio becomes slightly greater than 1. In the dawn flank, the lower-energy (<~100 keV) ion flux ratios show a reverse trend—ion fluxes are greater in the magnetosheath than in the magnetosphere, with a sharp boundary at the magnetopause. We do not know if such a reverse trend is real because light contamination can sometime appear and affect these lower energy channel counts.

Figure 6a shows the percentage of leakage of ions for low magnetic shear as solid lines (also within 0.3  $R_s$ ). Similar to electrons, the leakage is generally most pronounced in the dawn sector (blue line), followed by the dusk sector (red line), and least pronounced in the midday sector (green line). The leakage percentage trend is not monotonic, with the dawn flank being the least energy dependent, ranging around ~50% for all channels. The dawn-dusk ratio (Figure 6b), in general, decreases with increasing ion energies, from ~2 to 1. At high magnetic shear, the percentage of leakage shows little change at both the dawn and the dusk flanks for most of the energy channels. In the noon sector, the percentage of leakage decreases for the first three low energy channels, but increase for the rest of the higher-energy channels. The dawn-dusk asymmetry in the leakage is about the same for higher magnetic shear conditions, shown in Figure 6b as dotted lines, as for lower magnetic shear conditions. The dawn-dusk leakage ratio ranges from ~2.2 for the lowest energy channel A1 (27–35 keV) to ~1.1 for the highest energy channel A8 (3.5–4.0 MeV).

#### 4. Discussion

We have analyzed energetic (>20 keV) electron and ion data from the Cassini MIMI/LEMMS LET-C and LET-A channels, respectively. We focus on statistical characteristics of electron and ion fluxes in the vicinity of Saturn's magnetopause to gain insights into the physical process occurring at the magnetopause and the source of energetic particles in the magnetosheath.

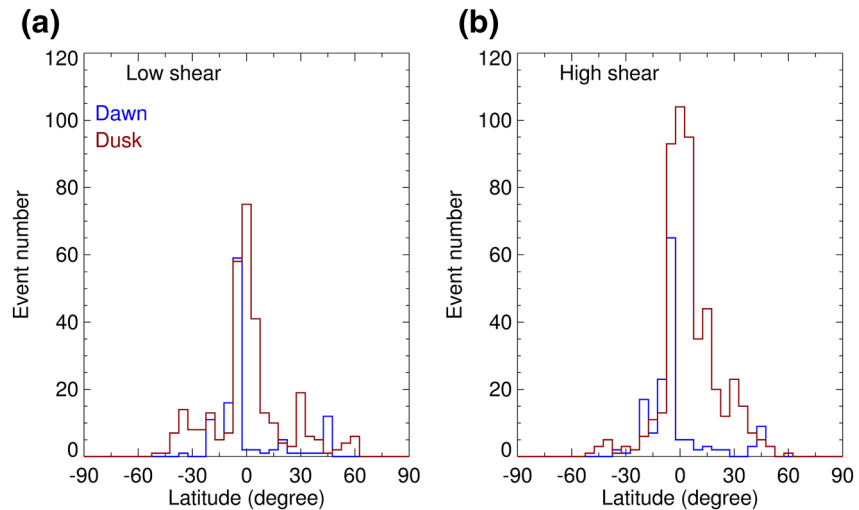


**Figure 7.** Normalized histograms of magnetopause crossing events under magnetic (a) low shear and (b) high shear conditions. In each panel, the blue, green, and red color is for the dawn, noon, and dusk sector, respectively. A  $5^\circ$  bin size is used to construct the histogram.

#### 4.1. Noon Maximum of Outer Magnetospheric Particle Flux

We will first discuss the noon flux maximum in the outer magnetosphere. The finding that electron and ion fluxes maximize in the local noon sector of Saturn's outer magnetosphere is not expected by the open drift shell theory, which predicts a dawn maximum for ions and dusk maximum for electrons. A possible explanation is sampling bias. According to Figure 2, the dusk sector magnetosheath was sampled in 2010–2013, which correspond to periods of increasing coronal mass ejection (CME) events, whereas the dawn sector magnetosheath was sampled in mixing periods, 2004–2007 and 2014–2017. During 2004–2007, which correspond to periods of increasing co-rotating interaction region/fast-stream, weaker but longer duration of magnetic activities are expected. The years of 2014–2017 are the first half of the descending phase of solar cycle 24. This could lead to different levels of solar energetic particle fluxes, along with a higher frequency of shock accelerated solar wind plasma reaching Saturn.

The solar wind dynamic pressure is inferred from the location of Saturn's magnetopause using the empirical magnetopause model (Kanani et al., 2010). The averaged dynamic pressure for the three local time sectors is estimated to be  $0.032 \pm 0.002$ ,  $0.301 \pm 0.268$ , and  $0.020 \pm 0.001$  nPa for the dawn, noon, and dusk sector, respectively. As such, there is a clear measurement bias in that our noon sector observations occurred during times of a more compressed magnetopause, which would explain the higher magnetospheric flux for the noon sector. The estimated dynamic pressure at the dawn and dusk sectors would suggest that the energetic particle flux should be larger at the dawn and smaller at dusk, which is not consistent with the measurement results. It may suggest that the sampling bias effect on the difference in the dawn-dusk energetic magnetosphere particle flux is probably small.

In addition, the time sampling bias also introduces a latitudinal sampling bias for the three sectors studied. This can also affect our statistical result because energetic particle fluxes peak at the equator. To explore this possibility, we plot the normalized latitudinal distribution of magnetopause crossing events in Figure 7. For the low-shear condition (Figure 7a), nearly all of the magnetopause crossings occurred within  $45^\circ$  from the equator, further justifying the latitudinal range chosen for our statistical study. In general, the distributions show a peak near the equator for all sectors, with a population mean of  $0.3^\circ$ ,  $8.9^\circ$ , and  $1.1^\circ$  for the dawn, noon, and dusk sector, respectively. The percentage of magnetopause crossing events within  $15^\circ$  from the equator for the dawn, noon, and dusk sector is 72%, 68%, and 67%, respectively. For the large magnetic shear condition (Figure 7b), the latitudinal coverage is very similar: the mean crossing latitude is  $-2.0$ ,  $9.1$ , and  $5.3$  for the dawn, noon, and dusk sector, respectively. The percentage of magnetopause crossing events within  $15^\circ$  from the equator for the dawn, noon, and dusk sector is 73%, 70%, and 79%, respectively. Therefore, the difference in the latitudinal sampling for the three sectors is small (within a few percent) and probably

would not contribute to the measured significant (a few times) difference on the energetic particle fluxes measured among these three sectors.

#### 4.2. Source of Energetic Particle Flux Enhancements

The bow shock has been considered as a source of energetic particles in a planetary magnetosheath, including Saturn's. One of the justifications for the bow shock source argument is that Saturn's bow shock is a high Mach number shock (Masters et al., 2013), which can accelerate particles to very high energies. The case study events on February 3, 2007, shown in Figure 1 also show existence of relativistic electrons at the bow shocks. Masters et al. (2013) interpreted these events as evidence of shock acceleration. Observations from CHEMS in Figure 1g show traces of water group ions accompanied with these energetic electrons, which would suggest at least some of the energetic ions at the bow shock were possibly of magnetospheric origin prior to being accelerated at the shock into the energy range of CHEMS. Furthermore, as the result of the Parker spiral field at Saturn being  $\sim 90^\circ$ , Saturn's bow shock is generally a quasiperpendicular shock across a large portion of the dayside, which favors multiple reflections of particles along the shock (Zank et al., 1996) or shock drift acceleration (e.g., Armstrong et al., 1985; Decker, 1988). These processes can accelerate both electrons and ions but cannot produce a dawn-dusk flux asymmetry as presented here. Lastly, Sergis et al. (2013) studied the compositional data acquired at Cassini between 2004 and 2011 and reported that the magnetosheath is comprised by low-energy (<few keV) particles from the shocked solar wind along with high-energy (>few keV) particles from the magnetosphere. Therefore, we may rule out the bow shock as the only source of energetic (> $\sim 20$  keV) particles in Saturn's magnetosheath observed LEMMS/LET.

Saturn's magnetosphere is populated with energetic (>10 keV) particles (e.g., Krimigis et al., 1981; N. E. Krupp et al., 2009). Especially given the observations of Sergis et al. (2013), it is expected that energetic particles can escape from Saturn's magnetosphere. As further evidence, solar wind-originating ions have been observed to gain access into the magnetosphere of Saturn, and as such, the same processes should allow for ions to escape (Allen et al., 2018). Indeed, the present study shows an inward positive gradient in the electron and ions (but weaker) differential flux across the entire dayside magnetopause (i.e., the energetic particle populations increase in flux from the magnetosheath to the magnetosphere). In addition, the enhanced flux in the magnetosheath at high magnetic shear also suggests that Saturn's magnetosphere may be a significant source of particles into the magnetosheath.

#### 4.3. Escape Mechanisms

In the previous section, we concluded that Saturn's magnetosphere is a source of energetic particles in the magnetosheath. Here we will discuss possible escape mechanisms that are supported by the present study. Energetic particles observed in the Earth's magnetosheath are often interpreted as a result of magnetic reconnection (Cohen et al., 2016; Korth et al., 1982; Mitchell et al., 1987) or the finite gyroradius effect (e.g., Sibeck & McEntire, 1988; Sibeck, McEntire, Lui, Lopez, & Krimigis, 1987; Sibeck, McEntire, Lui, Lopez, Krimigis, Decker, et al., 1987). Recent observations by the magnetospheric multiscale (MMS) suggest that both processes occur (e.g., Westlake et al., 2016).

Viscous interactions, particularly KH instabilities, are also a possible source of magnetospheric particle escape across the magnetopause, as well-developed KH vortices can lead to transient, small-scale reconnection between the magnetosheath and the magnetospheric field lines and so create a "mixing" layer that allows for the transfer of mass and momentum across the boundary. At the outer planets, and particularly at fast-rotators like Saturn, KHI has been shown by simple analytical formulations to be more likely to occur than dayside reconnection (Masters, 2018). All scenarios of particle escape must be investigated to determine what may be the dominant mechanism leading to magnetospheric energetic particles in Saturn's magnetosheath.

##### 4.3.1. Magnetic Field Reconnection and KH Instabilities

Reconnection between the interplanetary magnetic field with a planetary magnetosphere is a universal process, and has been observed at Saturn's magnetopause (e.g., Fuselier et al., 2014; McAndrews et al., 2008). Although it is not a major driver of Saturn's magnetospheric convection (Masters et al., 2014), magnetic



reconnection can still enable magnetospheric particles to leak out of the magnetosphere. When trapped particles enter into reconnection sites and exhausts, they gain energy as the particles stream along the newly opened magnetic field lines (Korth et al., 1979; Vines et al., 2017; Williams et al., 1979).

If particles escape the magnetosphere through magnetic reconnection, LEMMS should be able to observe the escape as long as they are within the LEMMS energy range. However, our case study of the magnetopause crossing at  $\sim 1200$  UT on February 3, 2007, shows a sharp energetic particle boundary occurred when the local magnetosheath magnetic field was strongly northward, favoring reconnection. However, it has been previously noted that the location of magnetic reconnection at Saturn is not directly comparable to what is expected at Earth due to diamagnetic drift (e.g., Desroche et al., 2013; Swisdak et al., 2003). In the magnetosphere, the peak flux on the C0 channel (20–30 keV) exceeds  $10^3 \text{ cm}^{-2}\text{sr}^{-1}\text{s}^{-1}\text{keV}^{-1}$ , whereas in the magnetosheath just outside the magnetosphere, the flux was  $\sim 1 \text{ cm}^{-2}\text{sr}^{-1}\text{s}^{-1}\text{keV}^{-1}$ , a three-order of magnitude difference. LEMMS did not observe escaping magnetospheric electrons. However, because Cassini was not rolling, the full pitch angles were not available to fully determine particle streaming direction. As such, a possible explanation is that Cassini was not viewing correct pitch angles to observe streaming particles. This interpretation is supported by the fact that LEMMS C was observing 90-degree particles (not field aligned) during this crossing. Another possibility is that magnetic reconnection may not occur even if magnetic field orientation favors reconnection, as the diamagnetic drift due to large changes in the plasma beta across the magnetopause can be great enough to suppress reconnection at low latitudes at Saturn (Desroche et al., 2013; Swisdak et al., 2003).

Evidence that supports magnetic reconnection is the transition of electron fluxes from the outer magnetosphere to the inner magnetosheath. The transition tends to be sharper for low magnetic shear and more gradual for high magnetic shear. However, this feature is most pronounced in the dusk sector, where dayside reconnection has been shown to be more favorable at lower latitudes (Desroche et al., 2013). Such a sharp flux transition is also observed for low-energy ions ( $< \sim 100$  keV) in the dusk sector at low magnetic shear and becomes gradual at high magnetic shear. In the dawn sector, we found little change in ion fluxes across the magnetopause at low magnetic shear and a sharp increase in ion flux ( $< \sim 250$  keV) at high magnetic shear. All these findings suggest that particle escape from the magnetosphere could be occurring through magnetic reconnection. The efficiency of electron escape due to reconnection can be roughly estimated as the difference in the percentage of leakage between high and low magnetic shear. Considering all particle energies, the averaged escape is  $\sim 11\%$  ( $\sim 9\%$ ) in the dawn flank,  $\sim 1\%$  ( $\sim 10\%$ ) in the noon sector, and  $\sim 20\%$  ( $\sim 17\%$ ) in the dusk flank for electrons (ions). These small values of percentage of leakage is consistent with the observations that dayside reconnection at Saturn's magnetopause is rare (Jasinski et al., 2016). Some have suggested that the high-beta plasma in Saturn's magnetosheath and large velocity shear at the magnetopause may inhibit reconnection at Saturn's magnetopause, especially at low latitudes (e.g., Desroche et al., 2013; Masters, Eastwood, et al., 2012).

Another dynamic process occurring at the magnetopause is the KH instability (KHI). Saturn's magnetopause, especially at the dawn flank, is susceptible to KHI because of the large flow shear in the outer magnetosphere due to its fast rotation. KHI has been observed at Saturn (e.g., Delamere et al., 2011; Masters, Achilleos, et al., 2012; Master et al., 2010; Wilson et al., 2012), and evidence of the occurrence of KH activity favors formation of KH waves in the postnoon to dusk sectors (Delamere et al., 2013; Desroche et al., 2013; Masters, Achilleos, et al., 2012) but are seen to mature into vortices on the dawn flank (Burkholder et al., 2017; Zhang et al., 2018). The development of "rolled-up" KH vortices may induce reconnection as suggested by numerical simulations (e.g., Eriksson et al., 2009; Ma et al., 2017; Nakamura et al., 2006, 2011, 2013; Zhang et al., 2018), and observations (Nakamura et al., 2017). Escape of magnetospheric particles can then occur at the KHI-induced reconnection sites. Global modeling of KHI for rotationally driven systems like Saturn have shown a distinct dawn-dusk asymmetry in the phase and propagation speed and size of the KH waves and resulting vortices (Ma et al., 2015; Walker et al., 2011; Zhang et al., 2018), which can lead to differences in the escape of magnetospheric plasma into the magnetosheath. This would allow for more "rolled-up" vortices to exist along the dawn-flank, and has previously been suggested as a possible mechanism for the interchange of plasma between the magnetosheath and magnetosphere (see Allen et al., 2018).

#### 4.3.2. Magnetospheric Leakage Due to Finite Gyroradius Effects

In addition to magnetic reconnection and KHI, escape of magnetospheric energetic particles is often explained in terms of magnetospheric "leakage," which is widely used to describe direct losses of

magnetospheric particles, upon encountering the magnetopause, to the magnetosheath. This can be due to finite gyroradius effects (e.g., Sibeck, McEntire, Lui, Lopez, Krimigis, Decker, et al., 1987), an outward magnetic gradient drift inside the magnetosphere (Keika et al., 2005; Kim et al., 2005), or various direct loss from the magnetosphere without invoking waves or magnetosheath structure (Mauk et al., 2016). These “leakage” processes allow some particles to exit (probably in a statistical sense) the magnetosphere when they encounter the magnetopause. The present findings, as shown in Figures 4 and 6, suggest that a large population of energetic particles in the magnetosheath were not likely not associated with magnetic reconnection, given the difference in the ratios for high shear angle versus low shear angle events. The ratio of magnetosheath electron (ion) fluxes associated with high shear to those with low shear (so possibly due to “leakage”) is 0.05 (0.5), 0.12 (0.4), and 0.25 (0.4) for the dawn, noon, and dusk sector, respectively. Therefore, magnetospheric “leakage” is a viable process responsible for the presence of energetic particles in Saturn’s magnetosheath, although the extent to which “leakage” due to finite gyroradius effects versus the role of KHI in actively allowing for particle escape requires further study.

The present study also shows a preference for enhanced magnetosheath fluxes of 10’s of keV electrons in the dawn flank, up to  $\sim 2$  times more than the dusk flank. However, the asymmetry reduces to  $\sim 50\%$  or less for higher energy particles. This local time asymmetry is likely related to the differences of magnetosheath populations seen in the dawn versus dusk flank by Burkholder et al. (2017). One other possibility is that the local time asymmetry in the LEMMS observations may suggest that the magnetopause becomes essentially “transparent” when the gyroradius of particles becomes large such that the magnetopause current layer and boundary layers are much smaller than the gyroradii of the energetic magnetospheric particles. The thickness of the current layer at Saturn’s low-latitude boundary layer has been estimated to be of order of  $1 R_s$  (Masters et al., 2011), which is much larger than the gyroradius of all electrons measured by the LEMMS-LET C channels (20–900 keV). Therefore, escape of electrons is not likely due to finite gyroradius effects. For protons with a gyroradius of  $1 R_s$  correspond to 800 keV (assuming  $|B| = 1.5$  nT on the magnetosheath side). We expect that escape of protons from the magnetosphere would occur for higher energy channels (A5–A8). Indeed, the percentage of proton leakage reaches the maximum at the A5 channel, as shown in Figure 6a. Recent observations and analytical modeling for both Earth and Jupiter have suggested that particles with gyroradii on the order of the current layer/boundary layer thickness are indeed more likely to escape the magnetosphere, rather than being entrained or simply diffusing across in a stochastic sense (Mauk et al., 2016, 2019). However, we cannot ignore the fact that the escape of both electrons and protons occurs at all energy channels. A multitude of escape processes must be at work. In the dawn flank, all A channels (25 keV–1.06 MeV ions) show little change at the magnetopause (Figure 5c). It may suggest that particles are more easily able to escape across the dawnside magnetopause, consistent with the findings of Burkholder et al. (2017).

#### 4.3.3. Charge Exchange

Another process that we will not develop significantly here is the escape through the conversion to energetic neutral atoms (ENAs). Since Saturn’s magnetosphere has been imaged via ENAs by the MIMI-Ion and Neutral Camera, we do know that energetic ions are converted to ENAs, which can then leave the system unimpeded by the magnetic and electric fields. These particles can be “stripped” in a number of ways and again become energetic ions, albeit at vastly different locations. We do not know the quantitative aspects of this process, but it may be an overlooked escape mechanism by which protons and heavy energetic ions can not only escape the magnetosphere but move into the upstream region in the solar wind before becoming ionized again. However, this process would not explain the slope (either gradual or steep) of energetic ions and electrons at the magnetopause.

## 5. Summary and Conclusions

We have conducted a distance-based superposed analysis on the LEMMS/LET-C channels for 20–900 keV electrons and the LEMMS/LET-A channels for 27–805 keV ions in the vicinity ( $\pm 1 R_s$ ) of the low-latitude (within  $45^\circ$ ) magnetopause in the dawn (05–10 LT), noon (10–14 LT), and dusk (14–19 LT) sectors. Our result can be summarized as follows.

1. The differential fluxes for energetic electrons (20–900 keV) in the magnetosheath near the magnetopause are smaller, by  $\sim 1$ – $2$  orders of magnitude in general, than their magnetospheric counterpart. The

- difference is much smaller ( $\sim 1$  order of magnitude or less) for energetic ions (27–1,600 keV), indicating that more energetic particles can more easily escape the magnetopause boundary
2. Differences in differential flux between the magnetosphere and the magnetosheath appear to be dependent upon energy and magnetic shear angle. In general, the difference reduces with increasing particle energies. The flux change across the magnetopause over all local times is sharper for low magnetic shear ( $< 30^\circ$ ) and more gradual for higher magnetic shear ( $> 60^\circ$ ), suggesting the occurrence of magnetic reconnection
  3. There is a dawn-dusk asymmetry in the energetic electron flux across the magnetopause. The flux change is sharp along the dusk flank and gradual along the dawn flank and the flux difference is more pronounced along the dusk flank than along the dawn flank. This may be related to differences in KHI development and likelihood of magnetic reconnection at the dawn versus dusk flank, as well as the differences in the background magnetosheath populations due to upstream process

### Data Availability Statement

The Cassini MIMI and MAG data reported herein are available through the NASA Planetary Data System (PDS) under the Cassini Programs at the website [pds.nasa.gov](https://pds.nasa.gov).

### Acknowledgments

We appreciate the use of the Cassini MIMI, CAPS, and mag data sets. Caitriona M. Jackman's work at Southampton is supported by STFC Ernest Rutherford Fellowship ST/L004399/1. Caitriona M. Jackman's work at DIAS is supported by Science Foundation Ireland grant 18/FRL/6199. NA was supported by the UK STFC Consolidated Grant (UCL/MSSL Solar and Planetary Physics, ST/N000722/1). This work was supported by a contract between Johns Hopkins University and NASA.

### References

- Allen, R. C., Livi, S. A., & Goldstein, J. (2016). Variations of oxygen charge state abundances in the global magnetosphere, as observed by Polar. *Journal of Geophysical Research: Space Physics*, *121*, 1091–1113. <https://doi.org/10.1002/2015JA021765>
- Allen, R. C., Livi, S. A., Vines, S. K., & Goldstein, J. (2016). Magnetic latitude dependence of oxygen charge states in the global magnetosphere: Insights into solar wind-originating ion injection. *Journal of Geophysical Research: Space Physics*, *121*, 9888–9912. <https://doi.org/10.1002/2016JA022925>
- Allen, R. C., Livi, S. A., Vines, S. K., Goldstein, J., Cohen, I., Fuselier, S. A., et al. (2017). Storm time empirical model of  $O^+$  and  $O^{6+}$  distributions in the magnetosphere. *Journal of Geophysical Research: Space Physics*, *122*, 8353–8374. <https://doi.org/10.1002/2017JA024245>
- Allen, R. C., Mitchell, D. G., Paranicas, C. P., Hamilton, D. C., Clark, G., Rymer, A. M., et al. (2018). Internal versus external sources of plasma at Saturn: Overview from Magnetospheric Imaging Investigation/Charge-Energy-Mass Spectrometer data. *Journal of Geophysical Research: Space Physics*, *123*, 4712–4727. <https://doi.org/10.1029/2018JA025262>
- Armstrong, T. P., Pesses, M. E., & Decker, R. B. (1985). Shock drift acceleration. In B. T. Tsurutani, & R. G. Stone (Eds.), *Collisionless shocks in the heliosphere: Reviews of current research*, Geophysical Monograph Series (Vol. 35, p. 271), American Geophysical Union, Washington D. C.
- Arridge, C. S., Jasinski, J. M., Achilleos, N., Bogdanova, Y. V., Bunce, E. J., Cowley, S. W. H., et al. (2016). Cassini observations of Saturn's southern polar cusp. *Journal of Geophysical Research: Space Physics*, *121*, 3006–3030. <https://doi.org/10.1002/2015JA021957>
- Baker, D. N., & Stone, E. C. (1977a). Observations of energetic electrons ( $E \geq 200$  keV) in the Earth's magnetotail: Plasma sheet and fireball observations. *Journal of Geophysical Research*, *82*(10), 1532–1546. <https://doi.org/10.1029/JA082i010p01532>
- Baker, D. N., & Stone, E. C. (1977b). The magnetopause electron layer along the distant magnetotail. *Geophysical Research Letters*, *4*(4), 133–136. <https://doi.org/10.1029/GL004i004p00133>
- Baker, D. N., & Stone, E. C. (1977c). The relationship of energy flow at the magnetopause to geomagnetic activity. *Geophysical Research Letters*, *4*(10), 395–398. <https://doi.org/10.1029/GL004i010p00395>
- Bridge, H. S., Belcher, J. W., Lazarus, A. J., Olbert, S., Sullivan, J. D., Bagenal, F., et al. (1981). Plasma observations near Saturn: Initial results from Voyager 1. *Science*, *212*, 217. <https://pubmed.ncbi.nlm.nih.gov/17783833/>
- Bridge, H. S., Bagenal, F., Belcher, J. W., Lazarus, A. J., & McNutt, R. L., (1982). Plasma observations near Saturn: Initial results from Voyager 2. *Science*, *215*(4532), 563–570. <https://doi.org/10.1126/science.215.4532.563>
- Burkholder, B., Delamere, P. A., Ma, X., Thomsen, M. F., Wilson, R. J., & Bagenal, F. (2017). Local time asymmetry of Saturn's magnetosheath flows. *Geophysical Research Letters*, *44*, 5877–5883. <https://doi.org/10.1002/2017GL073031>
- Cohen, I. J., Mauk, B. H., Anderson, B. J., Westlake, J. H., Sibeck, D. G., Giles, B. L., et al. (2016). Observations of energetic particle escape at the magnetopause: Early results from the MMS Energetic Ion Spectrometer (EIS). *Geophysical Research Letters*, *43*, 5960–5968. <https://doi.org/10.1002/2016GL068689>
- Cohen, I. J., Mauk, B. H., Anderson, B. J., Westlake, J. H., Sibeck, D. G., Turner, D., et al. (2017). Statistical analysis of MMS observations of energetic electron escape observed at/beyond the dayside magnetopause. *Journal of Geophysical Research: Space Physics*, *122*, 9440–9463. <https://doi.org/10.1002/2017JA024401>
- Decker, R. B. (1988). Computer modeling of test particle acceleration at oblique shocks. *Space Science Reviews*, *48*(3–4), 195–262.
- Delamere, P. A., Wilson, R. J., Eriksson, S., & Bagenal, F. (2013). Magnetic signatures of Kelvin-Helmholtz vortices on Saturn's magnetopause: Global survey. *Journal of Geophysical Research: Space Physics*, *118*, 393–404. <https://doi.org/10.1029/2012JA018197>
- Delamere, P. A., Wilson, R. J., & Masters, A. (2011). Kelvin-Helmholtz instability at Saturn's magnetopause: Hybrid simulations. *Journal of Geophysical Research*, *116*, A10222. <https://doi.org/10.1029/2011JA016724>
- Desroche, M., Bagenal, F., Delamere, P. A., & Erkaev, N. (2013). Conditions at the magnetopause of Saturn and implications for the solar wind interaction. *Journal of Geophysical Research: Space Physics*, *118*, 3087–3095. <https://doi.org/10.1002/jgra.50294>
- Dougherty, M. K., Kellock, S., Southwood, D. J., Balogh, A., Smith, E. J., Tsurutani, B. T., et al. (2004). The Cassini magnetic field investigation. *Space Science Reviews*, *114*, 331–383.
- Dougherty, M. K., Achilleos, N., Andre, N., Arridge, C. S., Balogh, A., Bertucci, C., et al. (2005). Cassini magnetometer observations during Saturn orbit insertion. *Science*, *307*(5713), 1266–1270. <https://doi.org/10.1126/science.1106098>

- Eriksson, S., Hasegawa, H., Teh, W.-L., Sonnerup, B. U. Ö., McFadden, J. P., Glassmeier, K.-H., et al. (2009). Magnetic island formation between large-scale flow vortices at an undulating postnoon magnetopause for northward interplanetary magnetic field. *Journal of Geophysical Research: Space Physics*, *114*(A1), A00C17. <http://dx.doi.org/10.1029/2008ja013505>
- Frank, L. A., Burek, B. G., Ackerson, K. L., Wolfe, J. H., & Mihalov, J. D. (1980). Plasmas in Saturn's magnetosphere. *Journal of Geophysical Research*, *85*(A11), 5695–5708. <https://doi.org/10.1029/JA085iA11p05695>
- Frank, L. A., & Van Allen, J. A. (1964). Measurements of energetic electrons in the vicinity of the sunward magnetospheric boundary with Explorer 14. *Journal of Geophysical Research*, *69*(23), 4923–4932. <https://doi.org/10.1029/JZ069i023p04923>
- Fuselier, S. A., Frahm, R., Lewis, W. S., Masters, A., Mukherjee, J., Petrinec, S. M., & Sillanpaa, I. J. (2014). The location of magnetic reconnection at Saturn's magnetopause: A comparison with Earth. *Journal of Geophysical Research: Space Physics*, *119*, 2563–2578. <https://doi.org/10.1002/2013JA019684>
- Hadid, L. Z., Sahraoui, F., Kiyani, K. H., Retinò, A., Modolo, R., Canu, P., et al. (2015). Nature of the MHD and kinetic scale turbulence in the magnetosheath of Saturn. *The Astrophysical Journal Letters*, *813*(2), L29. <https://doi.org/10.1088/2041-8205/813/2/L29>
- Jackman, C. M., Thomsen, M. F., & Dougherty, M. K. (2019). Survey of Saturn's magnetopause and bow shock positions over the entire Cassini mission: Boundary statistical properties and exploration of associated upstream conditions. *Journal of Geophysical Research: Space Physics*, *124*, 8865–8883. <https://doi.org/10.1029/2019JA026628>
- Jasinski, J. M., Arridge, C. S., Coates, A. J., Jones, G. H., Sergis, N., Thomsen, M. H., et al. (2016). Cassini plasma observations of Saturn's magnetospheric cusp. *Journal of Geophysical Research: Space Physics*, *121*(12), 12,047–12,067. <https://doi.org/10.1002/2016JA023310>
- Kanani, S. J., Hasegawa, H., Teh, W.-L., Sonnerup, B. U. Ö., McFadden, J. P., Glassmeier, K.-H., et al. (2010). A new form of Saturn's magnetopause using a dynamic pressure balance model, based on in situ, multi-instrument Cassini measurements. *Journal of Geophysical Research*, *115*, A06207. <https://doi.org/10.1029/2009JA014262>
- Keika, K., Nosé, M., Ohtani, S.-I., Takahashi, K., Christon, S. P., & McEntire, R. W. (2005). Outflow of energetic ions from the magnetosphere and its contribution to the decay of the storm time ring current. *Journal of Geophysical Research*, *110*, A09210. <https://doi.org/10.1029/2004JA010970>
- Kim, K. C., Lee, D.-Y., Lee, E. S., Choi, C. R., Kim, K. H., Moon, Y. J., et al. (2005). A new perspective on the role of the solar wind dynamic pressure in the ring current particle loss through the magnetopause. *Journal of Geophysical Research*, *110*, A09223. <https://doi.org/10.1029/2005JA011097>
- Korth, A., Kremser, G., Daly, P. W., & Amata, E. (1982). Observations of field-aligned energetic electron and ion distributions near the magnetopause at geosynchronous orbit. *Journal of Geophysical Research*, *87*(A12), 10413–10419.
- Korth, A., Kremser, G., Wilken, B., Amata, E., & Candidi, M. (1979). Variations of electron and ion distributions during dayside magnetopause crossings of GEOS-2. In B. Battrock, J. Mort, G. Haerendel, & J. Ortner (Eds.), *Magnetospheric Boundary Layers*. (Vol. 148, pp. 157–159). ESA Special Publication, France.
- Krimigis, S. M., Armstrong, T. P., Axford, W. I., Bostrom, C. O., Gloeckler, G., Keath, E. P., et al. (1981). Low-energy charged particles in Saturn's magnetosphere: Results from Voyager 1. *Science*, *212*(4491), 225–231. <https://doi.org/10.1126/science.212.4491.225>
- Krimigis, S. M., Mitchell, D. G., Hamilton, D. C., Livi, S., Dandouras, J., Jaskulek, S., et al. (2004). Magnetosphere Imaging Instrument (MIMI) on the Cassini Mission to Saturn. *Space Science Reviews*, *114*, 233–329.
- Krimigis, S. M., Venkatesan, D., Baricello, J. C., & Sarris, E. T. (1978). Simultaneous measurements of energetic protons and electrons in the distant magnetosheath, magnetotail, and upstream in the solar wind. *Geophysical Research Letters*, *5*(11), 961–964. <https://doi.org/10.1029/GL005i011p00961>
- Krupp, N. E., Lagg, A., Woch, J., Müller, A. L., Krimigis, S. M., Mitchell, D. G., et al. (2009). Energetic particles in Saturn's magnetosphere during the Cassini nominal mission. *Planetary and Space Science*, *57*(14–15), 1745–1768. <https://doi.org/10.1016/j.pss.2009.06.010>
- Krupp, N., Woch, J., Lagg, A., Espinosa, S. A., Livi, S., & Krimigis, S. M., et al. (2002). Leakage of energetic particles from Jupiter's dusk magnetosphere: Dual spacecraft observations. *Geophysical Research Letters*, *29*(15). <https://doi.org/10.1029/2001GL014290>
- Krupp, N., Woch, J., Lagg, A., Livi, S., Mitchell, D. G., Krimigis, S. M., et al. (2004). Energetic particle observations in the vicinity of Jupiter: Cassini MIMI/LEMMS results. *Journal of Geophysical Research*, *109*(A2), A09S10. <https://doi.org/10.1029/2003JA010111>
- Lai, H. R., Wei, H. Y., Russell, C. T., Arridge, C. S., & Dougherty, M. K. (2012). Reconnection at the magnetopause of Saturn: Perspective from FTE occurrence and magnetosphere size. *Journal of Geophysical Research*, *117*, A05222. <https://doi.org/10.1029/2011JA017263>
- Lazarus, A. J., & McNutt, R. L., Jr. (1983). Low-energy plasma ion observations in Saturn's magnetosphere. *Journal of Geophysical Research*, *88*(A11), 8831–8846. <https://doi.org/10.1029/JA088iA11p08831>
- Ma, X., Delamere, P., Otto, A., & Burkholder, B. (2017). Plasma transport driven by the three-dimensional Kelvin-Helmholtz instability. *Journal of Geophysical Research: Space Physics*, *122*, 10382–10395. <https://doi.org/10.1002/2017JA024394>
- Ma, X., Stauffer, B., Delamere, P. A., & Otto, A. (2015). Asymmetric Kelvin-Helmholtz propagation at Saturn's dayside magnetopause. *Journal of Geophysical Research: Space Physics*, *120*, 1867–1875. <https://doi.org/10.1002/2014JA020746>
- Masters, A. (2018). A more viscous-like solar wind interaction with all the giant planets. *Geophysical Research Letters*, *45*, 7320–7329. <https://doi.org/10.1029/2018GL078416>
- Masters, A., Achilleos, N., Cutler, J. C., Coates, A. J., Dougherty, M. K., & Jones, G. H. (2012). Surface waves on Saturn's magnetopause. *Planetary and Space Science*, *65*, 109–121. <https://doi.org/10.1016/j.pss.2012.02.007>
- Masters, A., Achilleos, N., Dougherty, M. K., Slavin, J. A., Hospodarsky, G. B., Arridge, C. S., & Coates, A. J. (2008). An empirical model of Saturn's bow shock: Cassini observations of shock location and shape. *Journal of Geophysical Research*, *113*, A10210. <https://doi.org/10.1029/2008JA013276>
- Masters, A., Eastwood, J. P., Swisdak, M., Thomsen, M. F., Russell, C. T., Sergis, N., et al. (2012). The importance of plasma  $\beta$  conditions for magnetic reconnection at Saturn's magnetopause. *Geophysical Research Letters*, *39*, L08103. <https://doi.org/10.1029/2012GL051372>
- Masters, A., Achilleos, N., Kivelson, M. G., Sergis, N., Dougherty, M. K., Thomsen, M. F., et al. (2010). Cassini observations of a Kelvin-Helmholtz vortex in Saturn's outer magnetosphere. *Journal of Geophysical Research*, *115*, A07225. <https://doi.org/10.1029/2010JA015351>
- Masters, A., Fujimoto, M., Hasegawa, H., Russell, C. T., Coates, A. J., & Dougherty, M. K. (2014). Can magnetopause reconnection drive Saturn's magnetosphere?. *Geophysical Research Letters*, *41*(6), 1862–1868. <https://doi.org/10.1002/2014GL059288>
- Masters, A., Mitchell, D. G., Coates, A. J., & Dougherty, M. K. (2011). Saturn's low-latitude boundary layer: 1. Properties and variability. *Journal of Geophysical Research*, *116*, A06210. <https://doi.org/10.1029/2010JA016421>
- Masters, A., Stawarz, L., Fujimoto, M., Schwartz, S. J., Sergis, N., Thomsen, M. F., et al. (2013). Electron acceleration to relativistic energies at a strong quasi-parallel shock wave. *Nature Physics*, *9*, 164–167. <https://doi.org/10.1038/NPHYS2541>
- Masters, A., Sulaiman, A. H., Stawarz, L., Reville, B., Sergis, N., Fujimoto, M., et al. (2017). An in situ comparison of energetic acceleration at collisionless shocks under differing upstream magnetic field orientations. *The Astrophysical Journal*, *843*(2), 147. <https://doi.org/10.3847/1538-4357/aa76ea>



- Mauk, B. H., Cohen, I. J., Haggerty, D. K., Hospodarsky, G. B., Connerney, J. E. P., Anderson, B. J., et al. (2019). Investigation of mass/charge-dependent escape of energetic ions across the magnetopauses of Earth and Jupiter. *Journal of Geophysical Research: Space Physics*, *124*, 5539–5567. <https://doi.org/10.1029/2019JA026626>
- Mauk, B. H., Cohen, I. J., Westlake, J. H., & Anderson, B. J. (2016). Modeling magnetospheric energetic particle escape across Earth's magnetopause as observed by the MMS mission. *Geophysical Research Letters*, *43*, 4081–4088. <https://doi.org/10.1002/2016GL068856>
- McAndrews, H. J., Owen, C. J., Thomsen, M., Lavraud, B., Coates, A., Dougherty, M., & Young, D. T. (2008). Evidence for reconnection at Saturn's magnetopause. *Journal of Geophysical Research*, *113*, A04210. <https://doi.org/10.1029/2007JA012581>
- McNutt, R. L., Jr., Haggerty, D. K., Hill, M. E., Krimigis, S. M., Livi, S., Ho, G. C., et al. (2007). Energetic particles in the Jovian magnetotail. *Science*, *318*(5848), 220–222. <https://doi.org/10.1126/science.1148025>
- Meng, C.-I., & Anderson, K. A. (1970). A layer of energetic electrons (>40 keV) near the magnetopause. *Journal of Geophysical Research*, *75*(10), 1827–1836. <https://doi.org/10.1029/JA075i010p01827>
- Meng, C.-I., & Anderson, K. A. (1975). Characteristics of the magnetopause energetic electron layer. *Journal of Geophysical Research*, *80*(31), 4237–4243. <https://doi.org/10.1029/JA080i031p04237>
- Mitchell, D. G., Kutchko, F., Williams, D. J., Eastman, T. E., Frank, L. A., & Russell, C. T. (1987). An extended study of the low-latitude boundary layer on the dawn and dusk flanks of the magnetosphere. *Journal of Geophysical Research*, *92*(A7), 7394–7404.
- Mitchell, D. G., Paranicas, C. P., Mauk, B. H., Roelof, E. C., & Krimigis, S. M. (2004). Energetic neutral atoms from Jupiter measured with the Cassini magnetospheric imaging instrument: Time dependence and composition. *Journal of Geophysical Research*, *109*, A09S11. <https://doi.org/10.1029/2003JA010120>
- Nakamura, T. K. M., Daughton, W., Karimabadi, H., & Eriksson, S. (2013). Three-dimensional dynamics of vortex-induced reconnection and comparison with THEMIS observations. *Journal of Geophysical Research: Space Physics*, *118*, 5742–5757. <https://doi.org/10.1002/jgra.50547>
- Nakamura, T. K. M., Eriksson, S., Hasegawa, H., Zenitani, S., Li, W. Y., Genestreti, K. J., et al. (2017). Mass and energy transfer across the Earth's magnetopause caused by vortex-induced reconnection. *Journal of Geophysical Research: Space Physics*, *122*, 11505–11522. <https://doi.org/10.1002/2017JA024346>
- Nakamura, T. K. M., Fujimoto, M., & Otto, A. (2006). Magnetic reconnection induced by weak Kelvin-Helmholtz instability and the formation of the low-latitude boundary layer. *Geophysical Research Letters*, *33*, L14106. <https://doi.org/10.1029/2006GL026318>
- Nakamura, T. K. M., Hasegawa, H., Shinohara, I., & Fujimoto, M. (2011). Evolution of an MHD-scale Kelvin-Helmholtz vortex accompanied by magnetic reconnection: two-dimensional particle simulations. *Journal of Geophysical Research*, *116*(A3), 3227. <https://doi.org/10.1029/2010JA016046>
- Ogasawara, K., Livi, S. A., Mitchell, D. G., Armstrong, T. P., & Krupp, N. (2011). Properties of energetic particle bursts at dawnside magnetosheath: Cassini observations during the 1999 Earth swing-by. *Journal of Geophysical Research*, *116*, A12207. <https://doi.org/10.1029/2011JA016813>
- Pilkington, N. M., Achilleos, N., Arridge, C. S., Guio, P., Masters, A., Ray, L. C., et al. (2015). Internally driven large-scale changes in the size of Saturn's magnetosphere. *Journal of Geophysical Research: Space Physics*, *120*, 7289–7306. <https://doi.org/10.1002/2015JA021290>
- Pilkington, N. M., Achilleos, N., Arridge, C. S., Masters, A., Sergis, N., Coates, A. J., & Dougherty, M. K. (2014). Polar confinement of Saturn's magnetosphere revealed by in situ Cassini observations. *Journal of Geophysical Research: Space Physics*, *119*, 2858–2875. <https://doi.org/10.1002/2014JA019774>
- Piša, D., Sulaiman, A. H., Santolik, O., Hospodarsky, G. B., Kurth, W. S., & Gurnett, D. A. (2018). First observation of lion roar emission in Saturn's magnetosheath. *Geophysical Research Letters*, *45*, 486–492. <https://doi.org/10.1002/2017GL075919>
- Richardson, J. D. (1986). Thermal ions at Saturn: Plasma parameters and implications. *Journal of Geophysical Research*, *91*(A2), 1381–1389. <https://doi.org/10.1029/JA091iA02p01381>
- Sarris, E. T., Krimigis, S. M., & Armstrong, T. P. (1976). Observations of magnetospheric bursts of high-energy protons and electrons at  $\sim 35 R_p$  with IMP 7. *Journal of Geophysical Research*, *81*(13), 2341–2355. <https://doi.org/10.1029/JA081i013p02341>
- Scholer, M., Daly, P. W., Paschmann, G., & Fritz, T. A. (1982). Field line topology determined by energetic particles during a possible magnetopause reconnection event. *Journal of Geophysical Research*, *87*(A8), 6073–6080. <https://doi.org/10.1029/JA087iA08p06073>
- Seidemann, P. K., Archinal, B. A., A'hearn, M. F., Conrad, A., Consolmagno, G. J., Hestroffer, D., et al. (2007). Report of the IAU/IAG Working Group on cartographic coordinates and rotational elements: 2006. *Celestial Mechanics and Dynamical Astronomy*, *98*, 155–180. <https://doi.org/10.1007/s10569-007-9072-y>
- Sergis, N., Jackman, C. M., Masters, A., Krimigis, S. M., Thomsen, M. F., Hamilton, D. C., et al. (2013). Particle and magnetic field properties of the Saturnian magnetosheath: Presence and upstream escape of hot magnetospheric plasma. *Journal of Geophysical Research: Space Physics*, *118*, 1620–1634. <https://doi.org/10.1002/jgra.50164>
- Sibeck, D. G., & McEntire, R. W. (1988). Multiple satellite observations of leakage of particles from the magnetosphere. *Advances in Space Research*, *8*(9–10), 201–216. [https://doi.org/10.1016/0273-1177\(88\)90133-0](https://doi.org/10.1016/0273-1177(88)90133-0)
- Sibeck, D. G., McEntire, R. W., Lui, A. T. Y., Lopez, R. E., & Krimigis, S. M. (1987). Magnetic field drift shell splitting: Cause of unusual dayside particle pitch angle distributions during storms and substorms. *Journal of Geophysical Research*, *92*(A12), 13485–13497. <https://doi.org/10.1029/JA092iA12p13485>
- Sibeck, D. G., McEntire, R. W., Lui, A. T. Y., Lopez, R. E., Krimigis, S. M., Decker, R. B., et al. (1987). Energetic magnetospheric ions at the dayside magnetopause: Leakage or merging? *Journal of Geophysical Research*, *92*(A11), 12097–12114. <https://doi.org/10.1029/JA092iA11p12097>
- Sittler, E. C., Jr., Ogilvie, K. W., & Scudder, J. D. (1983). Survey of low-energy plasma electrons in Saturn's magnetosphere: Voyagers 1 and 2. *Journal of Geophysical Research*, *88*(A11), 8847–8870. <https://doi.org/10.1029/JA088iA11p08847>
- Smith, H. T., Shappirio, M., Johnson, R. E., Reisenfeld, D., Sittler, E. C., Cray, F. J., et al. (2008). Enceladus: A potential source of ammonia products and molecular nitrogen for Saturn's magnetosphere. *Journal of Geophysical Research: Space Physics*, *113*(A11206). <https://doi.org/10.1029/2008JA013352>
- Sulaiman, A. H., Masters, A., Dougherty, M. K., & Jia, X. (2014). The magnetic structure of Saturn's magnetosheath. *Journal of Geophysical Research: Space Physics*, *119*, 5651–5661. <https://doi.org/10.1002/2014JA020019>
- Swisdak, M., Rogers, B. N., Drake, J. F., & Shay, M. A. (2003). Diamagnetic suppression of component magnetic reconnection at the magnetopause. *Journal of Geophysical Research*, *108*(A5), 1218. <https://doi.org/10.1029/2002JA009726>
- Thomsen, M. F., Coates, A. J., Jackman, C. M., Sergis, N., Jia, X., & Hansen, K. C. (2018). Survey of magnetosheath plasma properties at Saturn and inference of upstream flow conditions. *Journal of Geophysical Research: Space Physics*, *123*(3), 2034–2053. <https://doi.org/10.1002/2018JA025214>
- Vandergriff, J., DiFabio, R., Hamilton, D., Kusterer, M., Manweiler, J., Mitchell, D., et al. (2018). Cassini/MIMI instrument data user guide (NASA's Planetary System, Vol. 26). [https://pds-atmospheres.nmsu.edu/data\\_and\\_services/atmospheres\\_data/Cassini/inst-mimi.html](https://pds-atmospheres.nmsu.edu/data_and_services/atmospheres_data/Cassini/inst-mimi.html)

- Vines, S. K., Fuselier, S. A., Trattner, K. J., Burch, J. L., Allen, R. C., Petrinec, S. M., et al. (2017). Magnetospheric ion evolution across the low-latitude boundary layer separatrix. *Journal of Geophysical Research: Space Physics*, *122*, 10247–10262. <https://doi.org/10.1002/2017JA024061>
- Walker, R. J., Fukazawa, K., Ogino, T., & Morozoff, D. (2011). A simulation study of Kelvin-Helmholtz waves at Saturn's magnetopause. *Journal of Geophysical Research*, *116*, A03203. <https://doi.org/10.1029/2010JA015905>
- Westlake, J. H., Cohen, I. J., Mauk, B. H., Anderson, B. J., Mitchell, D. G., Gkioulidou, M., et al. (2016). The permeability of the magnetopause to a multispecies substorm injection of energetic particles. *Geophysical Research Letters*, *43*, 9453–9460. <https://doi.org/10.1002/2016GL070189>
- Williams, D. J., Fritz, T. A., Wilken, B., & Keppler, E. (1979). An energetic particle perspective of the magnetopause. *Journal of Geophysical Research*, *84*(A11), 6385–6396. <https://doi.org/10.1029/JA084iA11p06385>
- Wilson, R. J., Delamere, P. A., Bagenal, F., & Masters, A. (2012). Kelvin-Helmholtz instability at Saturn's magnetopause: Cassini ion data analysis. *Journal of Geophysical Research*, *117*, A03212. <https://doi.org/10.1029/2011JA016723>
- Wolfe, J. H., Mihalov, J. D., Collard, H. R., McKibbin, D. D., Frank, L. A., & Intriligator, D. S. (1980). Preliminary results on the Plasma environment of Saturn from the Pioneer 11 plasma analyzer experiment. *Science*, *207*, 403.
- Young, D. T., Berthelier, J. J., Blanc, M., Burch, J. L., Coates, A. J., Goldstein, R., et al. (2004). Cassini Plasma Spectrometer investigation. *Space Science Reviews*, *114*, 1–112. <https://doi.org/10.1007/s11214-004-1406-4>
- Zank, G. P., Pauls, H. L., Cairns, I. H., & Webb, G. M. (1996). Interstellar pickup ions and quasi-perpendicular shocks: Implications for the termination shock and interplanetary shocks. *Journal of Geophysical Research*, *101*(A1), 457–477. <https://doi.org/10.1029/95JA02860>
- Zhang, B., Delamere, P. A., Ma, X., Burkholder, B., Wiltberger, M., Lyon, J. G., et al. (2018). Asymmetric Kelvin-Helmholtz instability at Jupiter's magnetopause boundary: Implications for corotation-dominated systems. *Geophysical Research Letters*, *45*, 56–63. <https://doi.org/10.1002/2017GL076315>